International Journal of Geo-Information

MDPI

Article

Geographically-Informed Modeling and Analysis of Platform Attitude Jitter in GF-7 Sub-Meter Stereo Mapping Satellite

Haoran Xia [1], Xinming Tang [1,2,*], Fan Mo [2], Junfeng Xie [2] and Xiang Li [2]

[1] College of Geodesy and Geomatics, Shandong University of Science and Technology, Qingdao 266500, China; 202283020085@sdust.edu.cn
[2] Land Satellite Remote Sensing Application Center, MNR, Beijing 100080, China; mof@lasac.cn (F.M.); xiejf@lasac.cn (J.X.); 2021182130027@whu.edu.cn (X.L.)
* Correspondence: txm@lasac.cn

Abstract: The GF-7 satellite, China's inaugural sub-meter-level stereoscopic mapping satellite, has been deployed for a wide range of applications, including natural resource investigation, environmental monitoring, fundamental surveying, and the development of global geospatial information resources. The satellite's stable platform and reliable imaging systems are crucial for achieving high-quality imaging and precise attitude measurements. However, the satellite's operation is affected by both internal and external factors, which induce vibrations in the satellite platform, thereby affecting image quality and mapping accuracy. To address this challenge, this paper proposes a novel method for constructing a satellite platform vibration model based on geographic location information. The model is developed by integrating composite data from star sensors and gyroscopes (gyro) with subsatellite point location data. The experimental methodology involves the composite processing of gyro data and star sensor optical axis angles, integration of the processed data through time-matching and normalization, and denoising of the integrated data, followed by trigonometric fitting to capture the periodic characteristics of platform vibrations. The positions of the satellite substellar points are determined from the satellite orbit data. A rigorous geometric imaging model is then used to construct a vibration model with geographic location correlation in combination with the satellite subsatellite point positions. The experimental results demonstrate the following: (1) Over the same temporal range, there is a significant convergence in the waveform similarities between the gyro data and the star sensor optical axis angles, indicating a strong correlation in the jitter information; (2) The platform vibration exhibits a robust correlation with the satellite's geographic location along its orbit. Specifically, the model reveals that the GF-7 satellite experiences the maximum vibration amplitude between 5° S and 20° S latitude during its ascending phase, and the minimum vibration amplitude between 5° N and 20° N latitude during the descending phase. The model established in this study offers theoretical support for optimizing satellite attitude and mitigating platform vibrations.

Keywords: GF-7 satellite; platform vibration model; orbital period; geographic correlation

check for updates

Citation: Xia, H.; Tang, X.; Mo, F.; Xie, J.; Li, X. Geographically-Informed Modeling and Analysis of Platform Attitude Jitter in GF-7 Sub-Meter Stereo Mapping Satellite. *ISPRS Int. J. Geo-Inf.* **2024**, *13*, 413. https://doi.org/10.3390/ijgi13110413

Academic Editor: Wolfgang Kainz

Received: 3 September 2024
Revised: 10 November 2024
Accepted: 12 November 2024
Published: 15 November 2024

Copyright: © 2024 by the authors. Published by MDPI on behalf of the International Society for Photogrammetry and Remote Sensing. Licensee MDPI, Basel, Switzerland. This article is an open access article distributed under the terms and conditions of the Creative Commons Attribution (CC BY) license (https://creativecommons.org/licenses/by/4.0/).

1. Introduction

Satellites are typically affected by both internal factors, such as structural vibrations and control system instability, and external factors, including solar radiation pressure and gravity gradient torques, during their operational phases. These effects can induce vibrational phenomena on satellite platforms [1–3]. Although the magnitude of the vibrations generated by the satellite platform is generally small and unlikely to cause structural damage, more complex platform structures exhibit increased sensitivity to such vibrations. Therefore, the smaller the amplitude of the vibrations, the more challenging it becomes to achieve accurate measurements [4]. If the attitude changes induced by satellite platform vibrations are not adequately analyzed and addressed, they may have enduring repercussions on the geo-positioning and orientation of satellites equipped with high-resolution

cameras or those featuring complex platform structures. Furthermore, platform vibrations can have cumulative effects on satellite imagery, resulting in complications such as incoherent image stitching and diminished image quality [5,6]. These issues significantly hinder the effectiveness of satellites in applications related to natural resource assessment and geographic information infrastructure. Therefore, it is essential to conduct vibration detection and model development prior to the deployment of satellites for operational purposes, thereby providing the necessary technical support for the mitigation of vibrations on satellite platforms [7,8].

The investigation and analysis of satellite vibration have consistently been a significant concern within the domain of attitude dynamics and control. Organizations such as National Aeronautics and Space Administration (NASA) and European Space Agency have conducted extensive tests on satellite platform vibrations, revealing that factors such as mass distribution and structural materials are closely linked to platform flutter. Furthermore, the frequency of satellite attitude jitter predominantly resides in the low-frequency range [9,10]. Platform vibration is a complex phenomenon that is prevalent among high-resolution satellites, including QuickBird, Advanced Land Observing Satellite (ALOS), Pleiades, and various Chinese satellites such as the TH-1, ZY-3, and GF-1 satellites [11], all of which experience jitter [12–15]. A study conducted by Ayoub indicated that QuickBird is affected by a specific frequency of platform vibration, which results in geometric alterations in the captured images [16]. Hashimoto et al. [17] revealed that the calibration products of the ALOS Panchromatic Remote-sensing Instrument for Stereo Mapping (PRISM) camera sensor suffer from reduced accuracy in the rational polynomial coefficient model due to the effect of platform vibration. Amberg et al. [18] identified the platform vibration of the PLEIADES-HR satellite by analyzing adjacent band images from the multispectral sensor and subsequently performed in-orbit commissioning based on the jitter data. For the ZY-3 satellite, researchers from Tongji University, Wuhan University, and other institutions have conducted experiments to assess the vibration of the satellite platform. Their findings indicate a vibration frequency of approximately 0.6 Hz on the ZY-3 satellite platform, with the amplitude of vibration in the vertical orbit direction being greater than that in the orbital direction [19]. Tong et al. [20] proposed a comprehensive multi-sensor data processing method for detecting satellite vibration, which was utilized to analyze the variation patterns of vibration. The results demonstrated that the vibration frequency of the ZY-3 satellite remains within the range of 0.6~0.7 Hz. Liu et al. [21] introduced an attitude jitter detection method based on image analysis and dense ground control, validating the effectiveness of this method through an arithmetic example involving the ZY-3 satellite, with the detected vibration frequency approximating 0.65 Hz.

The GF-7 satellite represents China's inaugural sub-meter-class stereoscopic optical mapping satellite [22,23], equipped with a continuous operational capability of 24 h [24]. It fulfills the specifications for civilian stereo mapping at a scale of 1:10,000 [25] and is proficient in acquiring high-precision stereo elevation data [26], thereby significantly augmenting China's capacity to gather geographic information [27]. However, there remains a deficiency in comprehensive research concerning the detection of jitter periodicity and the development of a jitter model for the GF-7 satellite. Currently, the gyroscopes (gyro) employed can continuously provide three-axis angular rate data, which ensures a commendable real-time performance and high accuracy in relative attitude determination. However, a drift phenomenon is observed, leading to the gradual accumulation of integration errors and resulting in attitude dispersion. Conversely, star sensors are capable of delivering high-precision absolute attitude information, albeit at a lower operational frequency and with susceptibility to errors induced by radiation and other factors (Figure 1) [28,29]. To address these challenges, a joint detection scheme utilizing both star sensors and gyro is proposed. This approach leverages the high-precision attitude data from the star sensor to compensate for the relative attitude changes detected by the gyro, thereby achieving a complementary effect and facilitating the acquisition of high-precision jitter information. The orbital period of the GF-7 satellite is approximately 1.5 h, and its

platform flutter exhibits a certain correlation with this orbital period. Given that the satellite's orbit is intrinsically linked to its geographic location, this study aims to investigate the relationship between vibration and geographic location through a detailed analysis of the platform vibration and the orbital period. By utilizing original satellite gyro data and star sensor data, this research seeks to elucidate the patterns of satellite vibration and establish a vibration model that correlates with geographic location. This model will enable a mathematical linkage between platform vibration and the geographic location information of the satellite.

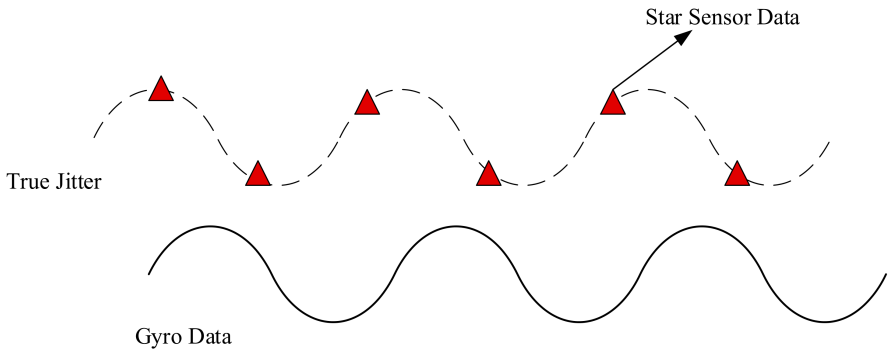


Figure 1. Comparative analysis of real and ideal vibration information from the star sensor and the gyro.

The overall structure of this paper is organized as follows. Section 1 reviews the research developments and challenges associated with satellite platform vibration modeling. In Section 2, the principles and workflow of the satellite platform vibration model construction method, which is based on geographic location information, are presented. Section 3 offers experimental data on satellite platform vibration and discusses the results of flutter tests conducted using GF-7 satellite attitude data. Finally, Section 4 summarizes the key conclusions and outlines the future work plan.

2. Materials and Methods

The GF-7 satellite is outfitted with a high-precision attitude measurement system that comprises advanced star sensors and three floating gyros [30]. Throughout the satellite's operational phase in orbit, real-time measurements of the satellite's attitude variations can be obtained. Additionally, data from the gyros and star sensors can be utilized to develop a geographically correlated vibration model in conjunction with the satellite's orbit. The specific technical methodology for constructing a geographically relevant vibration model using the vibration data from the GF-7 satellite is depicted in Figure 2.

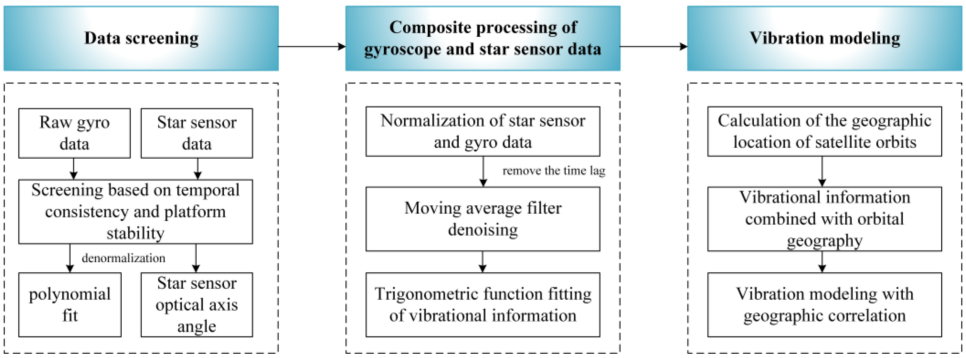


Figure 2. Flow chart for vibration modeling method of the GF-7 satellite.

The process comprises three steps: (1) The gyro data and star sensor data are filtered based on temporal consistency and platform stability to ensure the completeness and

validity of the test data; (2) The data are combined, and noise is mitigated through the application of a moving average filter, followed by trigonometric function fitting to analyze the vibration characteristics of the platform; (3) The flutter characteristics are correlated with the geographic location of the orbit, as determined using satellite orbit data, ultimately leading to the construction of a flutter model that incorporates geographic location correlation. The subsequent sections provide a comprehensive description of each step and the primary methods employed.

2.1. Data Screening

To ensure the reliability of the vibration test results for the satellite platform, it is imperative to first screen the experimental data to prevent the introduction of errors caused by anomalous data. Gyro and star sensor data are typically recorded in the form of time series. However, during satellite operation, these data may be affected by various factors, including noise, fluctuations in environmental conditions, motion interference, and data loss during transmission. These factors can lead to the occurrence of anomalous values or data loss in the downlink data. To address these issues, a method based on time consistency and stability is employed to filter the raw data effectively.

Gyro and star sensors integrate data at a predetermined sampling interval, thereby requiring that the time intervals between consecutive data points remain strictly consistent. In the event of data loss, this temporal consistency may be compromised, necessitating the removal or correction of erroneous data points.

In Figure 3, there are a total of N groups of data, with a neighboring data acquisition time interval of ΔT. The total acquisition time is represented by ΔT_N, while the number of acquired data points is N, multiplied by ΔT. It is only when all data points simultaneously satisfy Equation (1) that the track data can be recognized as continuous in time [31].

$$\begin{cases} T_{k+1} - T_k = \Delta T \\ T_N - T_1 = \Delta T_N \end{cases} \tag{1}$$

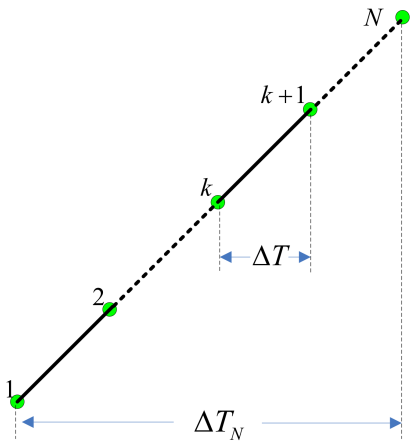


Figure 3. Time consistency analysis of gyro data and star sensor data.

The presence of unconventional forces and various other factors can lead to abnormal vibrations in satellite platforms, which may result in the acquisition of data that contain anomalies. Such irregularities can negatively affect the test results. To mitigate these adverse effects, this study imposes design stability constraints on the platform and mandate that the data adhere to the criteria for angular change stability. This approach aims to minimize input errors and enhance both the accuracy of the tests and the reliability of the modeling process.

$$s = \sqrt{\sum_{i=1}^{N} (g_i - g_{ave})^2} \tag{2}$$

where s is the platform stability as derived from gyro data; (i = 1, 2, 3, …, N) is the serial number associated with the gyro data; N is the total quantity of gyro data points; g_i represents the individual values of the gyro data; and g_{ave} is the mean value of the gyro dataset.

Based on Equation (2), when the stability of this set of gyro data exceeds the design threshold for platform stability (i.e., an empirical value that is 10 times greater), this dataset is unsuitable for jitter analysis and should be discarded.

2.2. Composite Analysis of Gyro and Star Sensor Data

Satellite gyros are subject to system drift, which can cause the output data to display both linear and nonlinear variations, thereby affecting the accuracy of attitude measurements. To better mitigate the effects of system drift, a fifth-order polynomial is used to fit the raw attitude data. This process enhances the accuracy of angular velocity measurements and supports more effective data analysis. The general form of the polynomial is presented in Equation (3):

$$f(x) = a_0 + a_1 x + \cdots + a_n x^n \tag{3}$$

where $f(x)$ is the fitting result; $a_0 \sim a_n$ is the fitting coefficient; and n is the fitting order.

Satellite star sensor data are represented using quaternions, which are a mathematical construct frequently employed to describe rotations in three-dimensional space. A quaternion comprises one real component and three imaginary components, and is expressed as follows:

$$q = w + xi + yj + zk \tag{4}$$

where w is the real part; x, y, and z are the real number; while i, j, and k are the unit imaginary number.

The utilization of two groups of star sensors can enhance the coverage of the field of view and improve the precision of attitude measurements. Additionally, the angle of the optical axis accurately reflects the rapid changes in attitude.

Consequently, the analysis of satellite jitter is conducted by calculating the optical axis angle using the quaternion representation of the two groups of star sensors. Given two unit quaternions q_1 and q_2, the dot product of q_1 and q_2 is defined as follows:

$$q_1 \cdot q_2 = w_1 w_2 + x_1 x_2 + y_1 y_2 + z_1 z_2 \tag{5}$$

where $q_1 = (w_1, x_1, y_1, z_1)$ and $q_2 = (w_2, x_2, y_2, z_2)$.

The angle θ between the optical axes of q_1 and q_2 is determined as follows:

$$\theta = 2\arccos\left(\frac{q_1 \cdot q_2}{\|q_1\|\|q_2\|}\right) \tag{6}$$

where $\|q_1\|$ and $\|q_2\|$ are the moduli of q_1 and q_2, respectively; while θ is the angle between the optical axes of the star sensor.

The positioning or orientation of the star sensors and gyro installation affects the measurement of attitude information. Variations in the value range of gyro attitude data can affect the effectiveness of data integration. To address this issue, a normalization method is employed to scale the star sensor data to align with the range of the gyro data, thereby ensuring consistency and comparability between the datasets. The integration of the data is achieved by calculating the average of the gyro data and the star sensor data within the same range. The relevant formula is expressed in Equation (7):

$$C = \left(\left(\left(\frac{A - \min(A)}{\max(A) - \min(A)}\right) \times (\max(G) - \min(G)) + \min(G)\right) + G\right) \times \frac{1}{2} \tag{7}$$

where C is the composite data; G is the gyro data; A is the optical-axis angle data; $min(G)$ and $min(A)$ are the minimum values of gyro and star sensor optical-axis angle data,

respectively; while $max(G)$ and $max(A)$ are the maximum values of gyro data and star sensor optical-axis angle data, respectively.

As the satellite transitions into and out of the Sun's shadow, it experiences significant temperature fluctuations. While the gyroscope, being housed within the satellite body, is minimally affected by these external temperature changes, the star sensor is more vulnerable due to its exposure. The onboard thermal control system is unable to rapidly stabilize the star sensor's temperature within the desired range, potentially leading to a time discrepancy between the gyroscope and star sensor data [32]. This discrepancy hinders the accurate integration of the two datasets. To address this issue, a time-matching method is employed to calculate and adjust for the time difference, thereby enabling precise data alignment and effective elimination of the temporal offset.

The process for eliminating the time difference is illustrated in Figure 4. By employing time-matching techniques, the corresponding time point in the star sensor data that aligns with T1 of the gyro data is identified. This process facilitates the determination of the time difference present in the star sensor data. Subsequently, the star sensor data are adjusted forward by this identified time difference to achieve temporal alignment between the datasets.

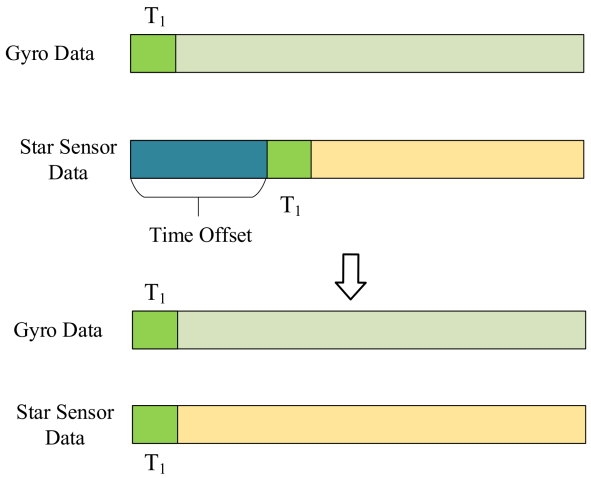


Figure 4. Time offset analysis in composite data from the gyro and star sensor. Time Offset is the temporal difference between the two datasets. T1 is a specific time point.

Compound data often contains noise that can adversely impact the results of the chattering test. Therefore, it is essential to eliminate this noise. The application of a moving average filter method involves utilizing a sliding window that incrementally traverses the data sequence at a predetermined step size, during which the values contained within the window are averaged. This technique effectively reduces noise and enhances data smoothness by averaging the values of data points within the sliding window. The corresponding equation is provided below.

$$y(n) = \frac{1}{N}\sum \frac{N-1}{k=0} x(n-k) \tag{8}$$

where $y(n)$ is the output signal; $x(n-k)$ is the input signal; N is the window size; and n is the step size.

In Figure 5, the purple curve denotes the original data, the green curve signifies the smoothed result, and the red box indicates the dimensions of the moving window.

To enhance the analysis of the frequency and periodicity characteristics of the composite signal, the denoised composite data are fitted using trigonometric functions. The trigonometric function model effectively captures both the periodic and fluctuating fea-

tures inherent in the data. For illustration, the sine function can be expressed by the following equation:

$$y(t) = A\sin(2\pi ft + \phi) + C \tag{9}$$

where $y(t)$ is the fitted value at time t; A is the amplitude;f is frequency; ϕ is the phase; and C is the offset.

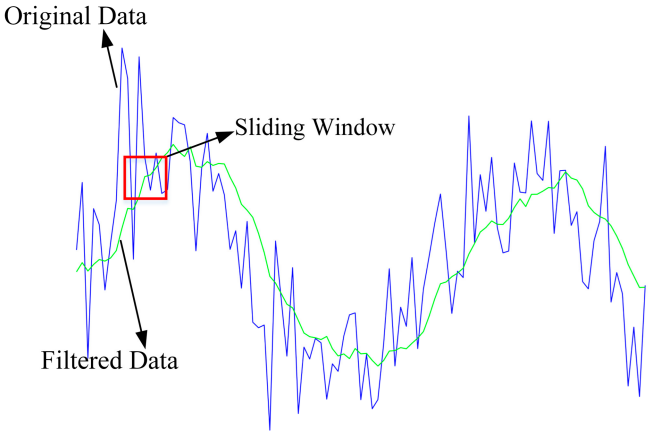


Figure 5. Schematic of the moving average filter.

2.3. Geographic Location-Dependent Flutter Modeling

The accurate determination of the geographic location of the substar point is essential for the development of a geographically correlated quivering model. The application of a rigorous geometric framework facilitates the precise identification of the subsatellite point's geographic coordinates, thereby providing critical data support for model developers. The orbit of a planetary hypocenter is a key factor affecting the position of the subsatellite point. Satellite orbital data typically encompass information regarding the satellite's position, velocity, and acceleration in space, often represented as a time series. The geographic coordinates of the satellite corresponding to the infra-planetary point are computed using the positional data recorded in the satellite's orbital information.

In Figure 6, the coordinate system labeled $O - X_1Y_1Z_1$ on the left represents the satellite body, whereas the coordinate system labeled $O - X_2Y_2Z_2$ on the right corresponds to the geodetic system. N and S are the North Pole and South Pole, respectively, while $P(B, L, H)$ is the geodetic coordinate that aligns with the satellite body coordinate.

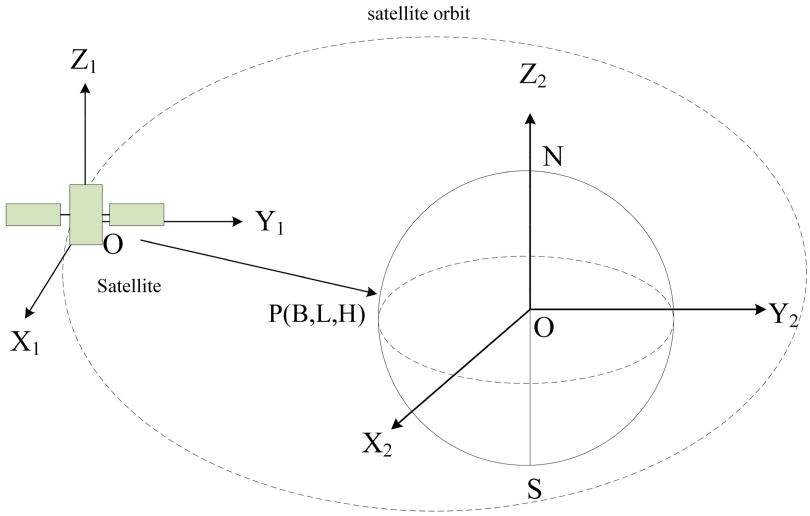


Figure 6. Satellite orbital data for calculating geographic locations of subsatellite points.

The trigonometric function serves as an effective tool for characterizing the phenomenon of periodic vibration. The phenomenon of chattering is often linked to periodic perturbations, which are observed as cyclical variations over time. As a result, the governing principles of satellite platform vibration are typically represented using a trigonometric function [33], as demonstrated in Equation (10):

$$V = a \sin\left(\frac{2\pi}{f} t + \theta\right) + l \tag{10}$$

It is essential to harmonize the presentation of vibrational information with the geographic location of satellite orbits. This can be accomplished by representing the geographic location information of the satellite orbit using trigonometric functions. Let y_1 represent the chatter frequency and y_2 represent the latitude of the geodetic coordinates corresponding to the geographic location of the orbital data. Therefore, y_1 and y_2 can be expressed as follows:

$$\begin{cases} y_1(t) = a_1 \sin(\omega_1 t + \theta_1) + l_1 \\ y_2(t) = a_2 \sin(\omega_1 t + \theta_2) + l_2 \end{cases} \tag{11}$$

where a_1 and a_2 are the amplitude of changes in amplitude and latitude, respectively; ω_1 and ω_2 are the factors related to the frequency of amplitude transformations and latitude changes, respectively; θ_1 and θ_2 are the phases of amplitude changes and latitude changes, respectively; l_1 and l_2 are the constants of amplitude and latitude changes; and t is the corresponding time of satellite operation, which can be determined as follows:

$$t = \frac{\arcsin\left(\frac{y_2(t) - l_2}{a_2}\right) - \theta_2}{\omega_2} \tag{12}$$

By substituting Equation (12) into Equation (11), a geographically correlated vibration model is derived as follows:

$$V = a_1 \sin\left(\frac{\omega_1}{\omega_2}\left(\arcsin(\frac{y_2 - l_2}{a_2}) - \theta_2\right) + \theta_1\right) + l_1 \tag{13}$$

3. Results

The GF-7 satellite is outfitted with four high-precision dual-field-of-view star sensors and three sets of gyros. Notably, the random drift of the three floating gyroscopes is less than $0.0006^\circ/\mathrm{h}$, allowing the relative attitude determination deviation of the satellite to be minimized to less than $0.2''$ within a specified time frame [34,35]. Specific technical specifications are shown in Table 1.

Table 1. Technical specifications of the GF-7 satellite attitude measurement system.

Typology		Parameters
Star Sensor	Star Sensors Combination	Two dual-field-of-view star sensors
	Accuracy	$1''$
	Frequency	8 Hz
Gyro	Model	8 Hz triple-floating gyro + 16 Hz fiber optic gyro
	Accuracy	$0.001^\circ/\mathrm{h}$

The objectives of the experiments are threefold: (1) to identify the attitude data that meet the requirements for the satellite platform vibration test; (2) to analyze the laws and characteristics of satellite vibrations using composite data; and (3) to develop a vibration model that correlates with geographic location.

3.1. Satellite Chatter Test Data Screening

Over extended durations, gyro may exhibit susceptibility to variations in linearity, a phenomenon commonly referred to as "drift." The occurrence of drift leads to a gradual divergence of data measurements from their true values. To mitigate the effects of linear variation, the gyroscope data can be fitted with a fifth-order polynomial according to Equation (3). Subsequently, the data are filtered based on temporal consistency and platform stability, with the results in Figure 7. The horizontal axis represents the number of gyroscope data points and the vertical axis is the raw gyroscope measurements in the form of angular velocity (°/s). This study presents the orbital data of the GF-7 satellite, encompassing orbit IDs 016396, 016416, 016431, and 016446, collected from 12 October 2022 to 15 October 2024. These data are depicted in Figure 7a–d. The data are recognized as being continuous in time without missing data when the data satisfy Equation (1), while the data stability needs to be much greater than the design value for platform stability. Following the assessment of data reliability, the one-orbit raw gyro data and star sensor data from 14 October 2022 (Figure 7c with ID 016431) were selected as the test data for jitter analysis and model construction.

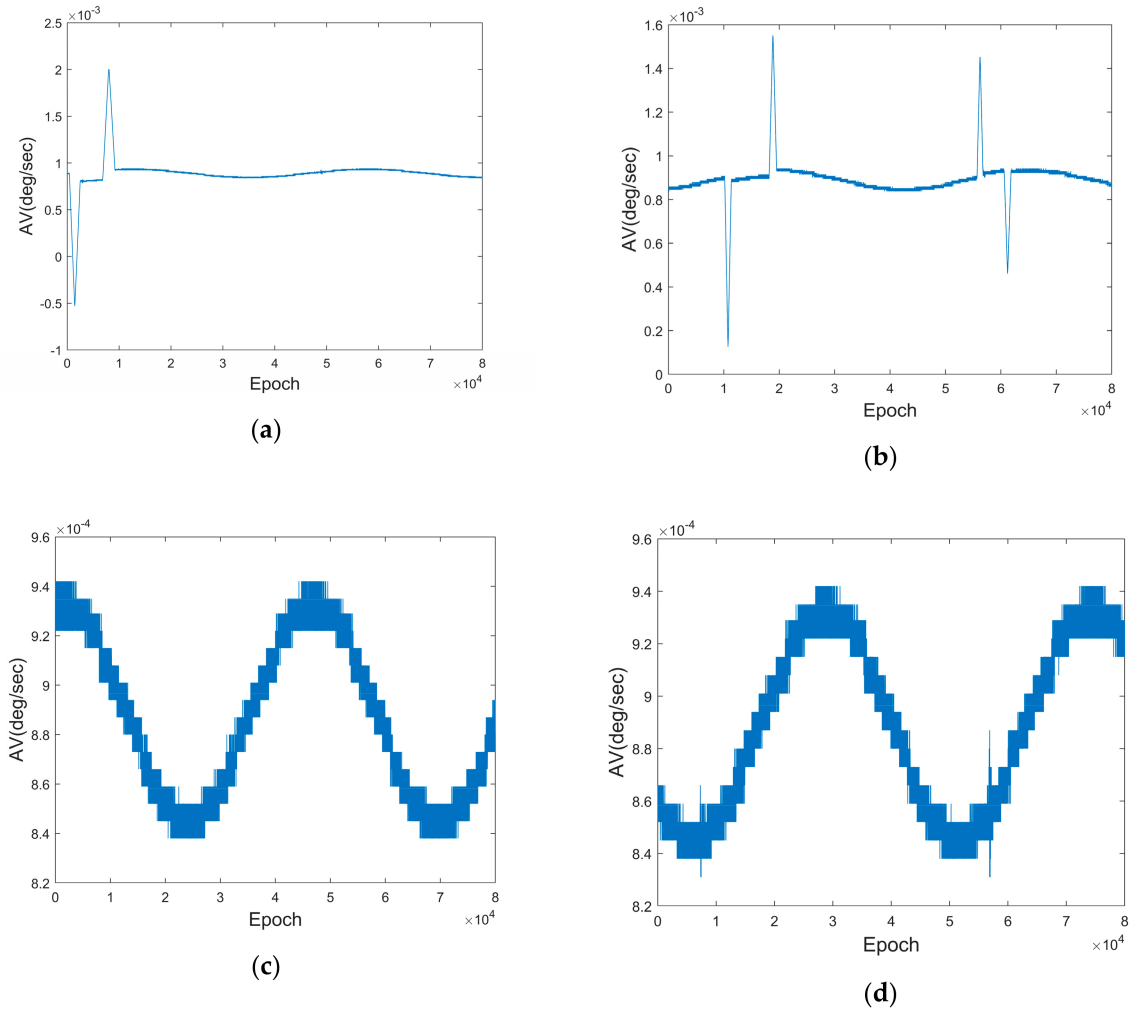


Figure 7. Filtered gyro data across multiple satellite tracks: (**a**) Track 016396; (**b**) Track 016416; (**c**) Track 016431; (**d**) Track 016446.

Figure 7a–d demonstrates a higher prevalence of notable outliers that do not conform to the established criteria for test data screening. The attitude data identified by the code 016431, recorded on 14 October 2022 (Figure 7c) has been selected for further analysis. The satellite platform exhibits a discernible periodic jitter, characterized by a sinusoidal

oscillation with a consistent amplitude. The jitter curve is characterized by low amplitude, high stability, and an average value of approximately 2.88″.

The GF-7 satellite's star sensors transmit attitude quaternion data, which are employed in this study to analyze the vibration of the satellite platform by calculating the boresight angles of the star sensors from two sets of quaternions. Initially, the star sensor data are filtered to ensure that the data quality meets the experimental requirements. The filtered star sensor data are then utilized to calculate the boresight angles in accordance with Equations (5) and (6). The results of the boresight angle calculations are presented in Figure 7.

The horizontal axis of Figure 8 represents the serial number of the data points, whereas the vertical axis denotes the angular value of the optical axis pinch angle measured in degrees. The angles of the star sensor boresight demonstrate periodic fluctuations. A comparative analysis of Figure 7 and 8 indicates that the waveform characteristics of the star sensor boresight angles align with those observed in the gyro data.

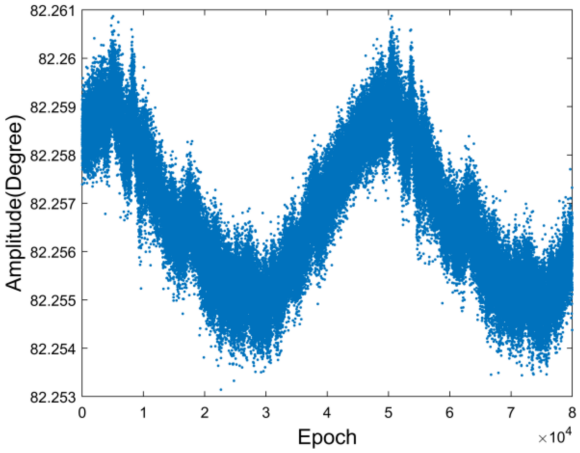


Figure 8. Optical axis clamping angle measurements from star sensor.

3.2. Composite Processing of Gyro-Star Sensor Data

To enhance the precision and reliability of satellite jitter detection and model construction, the integration of gyro data and star sensor boresight angle data is employed to improve the overall accuracy of data processing. The star sensor data reflects changes in the satellite's position relative to the stars, indicating relative variations. In contrast, the gyro data captures vibration information, which represents absolute changes. By applying proportional scaling through Equation (7), the relative changes identified by the star sensor data are converted into absolute changes, thereby facilitating the joint processing of the star sensor and gyro data. Additionally, since there is a time offset between the star-sensor optical axis angle and the gyro data, which affects the effect of data compositing, we match the same time point corresponding to the star-sensor optical axis angle based on the start time point of the gyro data, so as to calculate the time offsets between the star-sensor data and the gyro data and adjust the data range according to the offsets to ensure consistency between the time series of the two datasets. This adjustment is crucial for achieving accurate integration of the gyro data with the star sensor boresight angle data, given the inherent time offset between these two data sources.

The composite results are presented in Figure 9, where the horizontal axis denotes the number of data points and the vertical axis indicates the normalized resultant flutter amplitude. The composite data demonstrate a significant degree of overlap, with the data waveforms being nearly indistinguishable and exhibiting identical chirp periods. Furthermore, the graph reveals noticeable noise components, which must be eliminated to avoid the potential contamination of the test inspection results with extraneous noise.

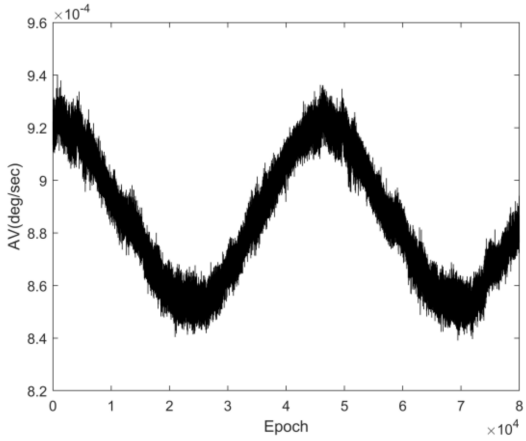


Figure 9. Composite analysis of gyro and star sensor pinch angle data.

To mitigate the effect of noise in the data, the moving average filtering method (Equation (8)) is utilized. The sliding window size is established at 10, and the resultant output is depicted in Figure 10.

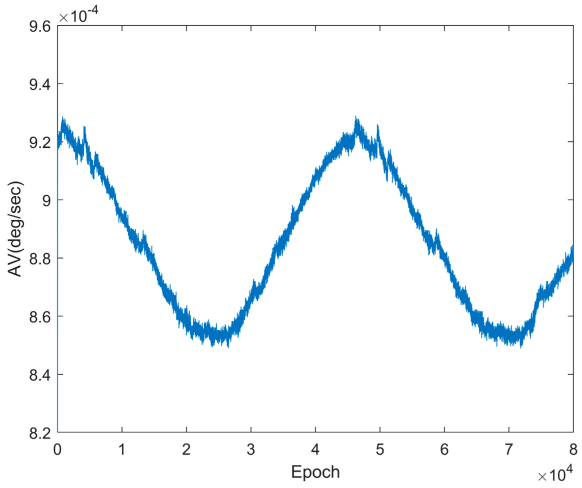


Figure 10. Denoising results using moving average filter.

In Figure 10, the horizontal axis represents the quantity of gyro data, while the vertical axis denotes the gyro data values measured in degrees per second. In Figure 9, the waveform graph exhibits a smoother and more precise representation, with the periodicity feature being more pronounced.

To more accurately characterize the oscillations of the platform, the sine function presented in Equation (9) is employed to fit a trigonometric function to the waveform map obtained from the post-inverse Fourier transformation. This approach facilitates the extraction of the primary periodic components.

The results are illustrated in Figure 11. The frequency of the fitted function corresponds to the period of the chattering vibration, and the fitted curve demonstrates a high degree of consistency with the actual signal, indicating a favorable fitting effect. Analysis of the coefficients of the fitted curve revealed that there were approximately 4.5×10^4 data points within a complete chirp cycle. Considering that the sampling frequency of the gyro was 8 Hz, the chirp cycle of the satellite platform was estimated to be approximately 1.5 h, which aligns with the duration required for the satellite to complete one full operational cycle.

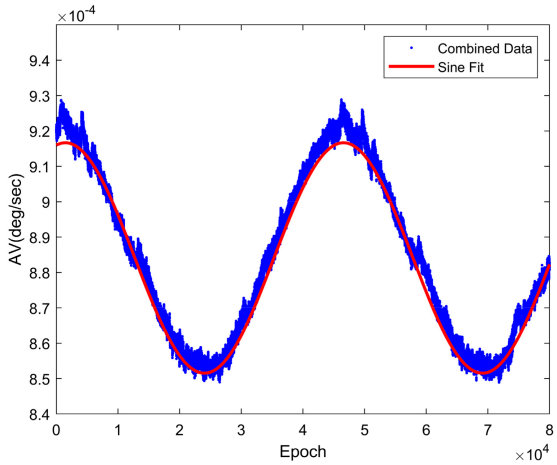


Figure 11. Results of trigonometric function fitting for vibration data analysis. The blue color indicates composite data. The red curve represents the fitted result.

3.3. Calculating the Geographic Location of Satellite Orbits

To ascertain the geographic position of a satellite, it is essential to first calculate the Beijing time corresponding to the satellite's operational period. This calculation is accomplished by utilizing the time code information embedded within the attitude data. The next step involves correlating this calculated time with the time sequence of the satellite's orbital data. This process enables the determination of the satellite's position at a specific standard time. Ultimately, the precise positional data, originally expressed in the body coordinate system, is converted into a format compatible with the geodetic coordinate system. The resulting data are presented in Figure 12.

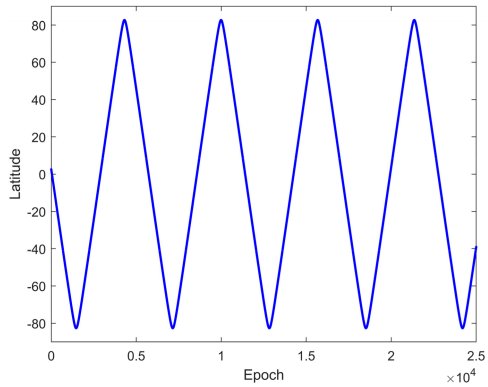


Figure 12. Geographic distribution of satellite orbital paths.

Figure 12 illustrates the serial number of the dataset on the horizontal axis and latitude on the vertical axis. The operational orbit of the GF-7 satellite is positioned between 80° N and 80° S latitude. The ascending phase of the satellite's orbit occurs between 80° S latitude and 80° N latitude, whereas the descending phase transpires between 80° N latitude and 80° S latitude.

In an effort to harmonize the representation of vibration information with the geographic location of the satellite orbit, the geographic location of the satellite orbit is modeled using Equation (9).

3.4. Modeling of Flutter Vibration

The results of applying trigonometric functions to model the relationship between flutter and geographic location are outlined in Table 2.

Table 2. Fitting results correlating satellite vibrating (chattering) with geographic location.

Trigonometric Coefficient	y_1	y_2
a	71.44	3.274×10^{-5}
b	1.106×10^{-3}	1.384×10^{-4}
c	−3.202	1.411

where y_1 is the fitting result of the composite data; y_2 is the fitting result of the geographic position of the satellite orbit; a is the amplitude of the fitted function; b is the angular frequency of the function; and c is the phase.

The fitting function of the composite data exhibits a mathematical correlation with the fitting results of the satellite orbit data, thereby facilitating the development of a flutter model for the GF-7 satellite. The resultant vibration model, which incorporates a geographic location correlation, is presented as follows:

$$y_2 = 3.274 \times 10^{-5} \sin(0.2514 \arcsin\left(\frac{y_1}{71.44}\right) + 1.817) \quad (14)$$

According to Equation (14), the variation in satellite chattering as a function of latitude is depicted in Figure 13.

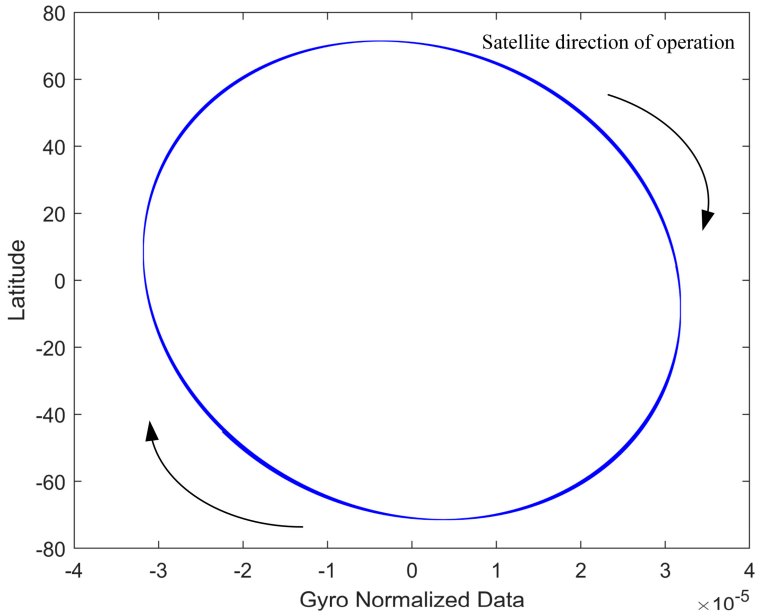


Figure 13. Variations in satellite flutter amplitude relative to geographic location.

In Figure 13, the horizontal axis represents the normalized values of the composite data, while the vertical axis indicates the latitude of the geographic locations corresponding to the satellite's operational orbit. The orientation of the arrow signifies the direction of satellite operation. During the ascending phase of the orbit, the satellite platform experiences the highest levels of vibration at latitudes of 5° S and 20° S. In contrast, during the descending phase, the lowest levels of vibration are recorded at latitudes ranging from 5° N to 20° N.

4. Discussion

Regarding the composite processing of star sensor gyro data, the comparative analysis in Figures 7 and 8 indicates a significant convergence between the gyro signal waveform and the star sensor optical axis angle waveform, both exhibiting similar characteristics and trends in variation. The primary characteristic points are largely consistent across both datasets. Given that the star sensor provides relative information while the gyro data offer absolute information, it is essential to composite the gyro data with the star sensor optical axis angle through a proportional scaling process to convert the relative information

into absolute information for effective star sensor/gyro joint jitter detection. However, a temporal discrepancy exists between the star tracker and gyro data, which hinders the potential for accurate compositing. This discrepancy may be attributed to the satellite's periodic transitions into and out of solar shadow, significant temperature fluctuations, and the thermal environment affecting the star sensor. Additionally, the onboard thermal control system's inability to rapidly adjust the star sensor's temperature within the specified range may further exacerbate this discrepancy. As a result, a time lag is observed between the gyro and star sensor data. The time difference is determined using a time-matching method, and the data are accurately composited by applying a phase shift to the star sensor data. The resulting composite is illustrated in Figure 9.

Composite data frequency domain denoising is presented in this study. The composite data in Figure 9 contains a noisy signal, which was processed using a moving average smoothing filter to eliminate the noise components. A trigonometric function was utilized to model the composite data, and the results of this fitting process are depicted in Figure 11. The trigonometric function provided an optimal fit to the data, effectively capturing the underlying trend of the composite dataset. This result supports the conclusion that the satellite platform exhibited a discernible periodicity in its chattering behavior, with a periodicity of approximately 1.5 h.

Regarding the development of a geographic correlation chatter model, in Figures 11 and 12, a correlation exists between the vibrations of the GF-7 satellite and the latitude of its geographic orbit. A geographically correlated periodic vibration model has been established based on this relationship, indicating that the magnitude of the vibration amplitude varies with changes in latitude. The variations in chattering at different latitudes (Figure 13) are derived from the vibration model. Throughout a complete operational cycle of the satellite, the chattering amplitude reaches its maximum between 5° S and 20° S latitude during the ascent phase of the orbit. Conversely, the chattering amplitude attains its minimum when the satellite operates between 5° N and 20° N latitude during the descent phase of the orbit. The results of the above research and the establishment of the vibration model can be used to investigate the effects of vibration on the imaging system and optimize the operating attitude of the satellite platform, so as to effectively improve the clarity of the image and the accuracy of the remote-sensing data. In addition, it can also provide support for the optimization of satellite design.

5. Conclusions

This study presents a method for constructing a satellite platform vibration model based on geographic location information, utilizing composite data from the GF-7 satellite's gyro and star sensor for jitter detection. Initially, the filtered satellite attitude data are normalized to align with the range of the gyroscope data and accurately composited based on time offsets. Subsequently, noise is removed using a moving average filter, ensuring the validity and accuracy of the vibration detection experiment. Finally, the relationship between the data fitting results and the satellite orbit data is analyzed, revealing the periodic characteristics of satellite jitter and leading to the establishment of a vibration model with geographic location correlation. The study yields the following key conclusions:

(1) The application of trigonometric functions allows for a more precise alignment with the vibration data of the GF-7 satellite, enabling the effective extraction of vibration characteristics, with a recorded vibration amplitude of approximately 2.88″.
(2) A comparison between the gyro data and the cyclic characteristics of the star sensor boresight angle confirms that the GF-7 satellite platform exhibits periodic vibration behavior. The vibration period corresponds with the satellite's complete operational cycle, approximately 1.5 h.
(3) The evidence suggests a correlation between the satellite platform's vibration and its orbital path. During a full operational cycle, the satellite experiences its maximum vibration amplitude, reaching 9.182×10^{-4}°/s, within the 5° S to 20° S latitude range during its ascending phase. Conversely, the minimum vibration amplitude,

recorded at 8.541×10^{-4}°/s, occurs within the 5° N to 20° N latitude range during the descending phase.

The results indicate that the flutter of the GF-7 satellite platform may be affected by the Earth's gravity field distribution and changes in the satellite's orbital elevation. Future research will delve deeper into the underlying causes of the vibrations observed in the GF-7 satellite. The study will also conduct annual cycle frequency analyses, comprehensively analyze the jitter phenomenon, and refine the vibration model. The study found that the correlation between vibration and geographic location provides a reference for satellite operation, especially for the optimization of vibration control for specific orbital segments, which can further improve the quality of remote-sensing data.

Author Contributions: Xinming Tang, Haoran Xia and Junfeng Xie designed the study; Haoran Xia and Xiang Li processed the data; Haoran Xia and Fan Mo analyzed the data and wrote the paper. All authors have read and agreed to the published version of the manuscript.

Funding: This research was funded by the National Natural Science Foundation of China (42001416). Key Laboratory of China-ASEAN Satellite Remote-Sensing Applications, Ministry of Natural Resources of the People's Republic of China (ZDMY202302), and Technology Innovation Center for Spatio-temporal Information and Equipment of Intelligent City, MNR (No. STIEIC-KF202308). Nat-ural Science Foundation of Shandong Province (No. ZR2022QD141).

Data Availability Statement: The data presented in this study are available on request from the corresponding author due to data confidentiality.

Conflicts of Interest: The authors declare no conflicts of interest.

References

1. Johnston, J.D.; Thornton, E.A. Thermally induced dynamics of satellite solar panels. *J. Spacecr. Rocket.* **2000**, *37*, 604–613. [CrossRef]
2. Teshima, Y.; Iwasaki, A. Correction of attitude fluctuation of terra spacecraft using ASTER/SWIR imagery with parallax observation. *IEEE Trans. Geosci. Remote Sens.* **2007**, *46*, 222–227. [CrossRef]
3. Wang, Y.; Dong, Z.; Wang, M. Attitude low-frequency error spatiotemporal compensation method for VIMS imagery of gaofen-5B satellite. *IEEE Geosci. Remote Sens. Lett.* **2024**, *21*, 6004205. [CrossRef]
4. Sun, Y. Study of the Effect of in-Orbit Chattering of Satellite Platforms on the Image Quality of High-Resolution Remote Sensors. Master's Thesis, Chinese Academy of Sciences (Changchun Institute of Optical Precision Machinery and Physics), Changchun, China, 2013.
5. Deng, Q. Study on the Effect of Satellite Chatter on Remote Sensing Image Quality and Experimental Validation. Master's Thesis, Zhejiang University, Hangzhou, China, 2013.
6. Sun, T.; Long, H.; Liu, B.C.; Li, Y. Application of attitude jitter detection based on short-time asynchronous images and compensation methods for Chinese mapping satellite-1. *Opt. Express* **2015**, *23*, 1395–1410. [CrossRef] [PubMed]
7. Kirk, R.L.; Howington-Kraus, E.; Redding, B.; Galuszka, D.; Hare, T.M.; Archinal, B.A.; Soderblom, L.A.; Barrett, J.M. High-resolution topomapping of candidate MER landing sites with Mars Orbiter Camera narrow-angle images. *J. Geophys. Res. Planets* **2003**, *108*. [CrossRef]
8. Tong, X.; Ye, Z.; Xu, Y.; Tang, X.; Liu, S.; Li, L.; Xie, H.; Wang, F.; Li, T.; Hong, Z. Framework of jitter detection and compensation for high resolution satellites. *Remote Sens.* **2014**, *6*, 3944–3964. [CrossRef]
9. Toyoshima, M.; Araki, K. In-orbit measurements of short-term attitude and vibrational environment on the Engineering Test Satellite VI using laser communication equipment. *Opt. Eng.* **2001**, *40*, 827–832.
10. Lieber, M.D. Space-Based Optical System Performance Evaluation with Integrated Modeling Tools. In Proceedings of the Modeling, Simulation, and Calibration of Space-Based Systems, Orlando, FL, USA, 12–16 April 2004; SPIE: Washington, DC, USA, 2004.
11. Pan, J.; Zhu, Y.; Song, X.; Hu, F.; Zhang, C.; Wang, M. Jitter detection and image restoration based on continue dynamic shooting model for high-resolution TDI CCD satellite images. *IEEE Trans. Geosci. Remote Sens.* **2021**, *59*, 4915–4933. [CrossRef]
12. Wang, M.; Zhu, Y.; Jin, S.; Pan, J.; Zhu, Q. Correction of ZY-3 image distortion caused by satellite jitter via virtual steady reimaging using attitude data. *ISPRS J. Photogramm. Remote Sens.* **2016**, *119*, 108–123. [CrossRef]
13. Wang, M.; Zhu, Y.; Pan, J.; Yang, B.; Zhu, Q. Satellite jitter detection and compensation using multispectral imagery. *Remote Sens. Lett.* **2016**, *7*, 513–522. [CrossRef]
14. Tang, X.; Xie, J.; Zhu, H.; Mo, F. Overview of Earth Observation Satellite Platform Microvibration Detection Methods. *Sensors* **2020**, *20*, 736. [CrossRef]

15. Ye, Z.; Xu, Y.; Tong, X.; Zheng, S.; Zhang, H.; Xie, H.; Stilla, U. Estimation and analysis of along-track attitude jitter of ZiYuan-3 satellite based on relative residuals of tri-band multispectral imagery. *ISPRS J. Photogramm. Remote Sens.* **2019**, *158*, 188–200. [CrossRef]
16. Ayoub, F.; Leprince, S.; Binet, R.; Lewis, K.W.; Aharonson, O.; Avouac, J.P. Influence of Camera Distortions on Satellite Image Registration and Change Detection Applications. In Proceedings of the IGARSS 2008—2008 IEEE International Geoscience and Remote Sensing Symposium, Boston, MA, USA, 7–11 July 2008; IEEE: Piscataway, NJ, USA, 2008.
17. Igarashi, T.; Shimada, M.; Rosenqvist, A.; Hashimoto, T.; Tadono, T.; Matsuoka, M.; Yamamoto, H. Preliminary study on data sets of ADEOS-II and ALOS dedicated to terrestrial carbon observation. *Adv. Space Res.* **2003**, *32*, 2147–2152. [CrossRef]
18. Amberg, V.; Dechoz, C.; Bernard, L.; Greslou, D.; Lussy, F.D.; Lebegue, L. In-Flight Attitude Perturbances Estimation: Application to PLEIADES-HR Satellites. In Proceedings of the Earth Observing Systems XVIII, San Diego, CA, USA, 27–30 August 2013; SPIE: Washington, DC, USA, 2013.
19. Zhu, Y.; Wang, M.; Pan, J.; Hu, F. Detection of Resource 3 platform tremor using multispectral imagery. *Acta Geod. Cartogr. Sin.* **2015**, *44*, 399–406+413.
20. Tong, X.H.; Ye, Z.; Liu, S.J. Key Technical Methods and Applications of High-Resolution Satellite Flutter Detection Compensation. *Acta Geod. Cartogr. Sin.* **2017**, *46*, 1500–1508.
21. Liu, S.; Tong, X.; Wang, F.; Sun, W.; Guo, C.; Ye, Z.; Jin, Y.; Xie, H.; Chen, P. Attitude Jitter Detection Based on Remotely Sensed Images and Dense Ground Controls: A Case Study for Chinese ZY-3 Satellite. *IEEE J. Sel. Top. Appl. Earth Obs. Remote Sens.* **2016**, *9*, 5760–5766. [CrossRef]
22. Li, Q. Successful launch of "GF-7" satellite by "Long March" 4B carrier rocket. *Aero Chin.* **2019**, *11*, 23.
23. Tang, X.; Zhu, X.; Hu, W.; Ding, J. Geometric Accuracy Analysis of Regional Block Adjustment Using GF-7 Stereo Images without GCPs. *Remote Sens.* **2023**, *15*, 2552. [CrossRef]
24. Lv, Z.; Lei, Y. *Satellite Attitude Measurement and Determination*; National Defense Industry Press: Beijing, China, 2013; pp. 71–79.
25. Cao, H.; Zhang, X.; Zhao, C.; Xu, C.; Mo, F.; Dai, J. Overall design and technological innovation of GF-7 satellite. *Chin. Space Sci. Technol.* **2020**, *40*, 1.
26. Li, D.; Sui, Z.; Long, X.; Li, Q.; Qiao, Z.; Zhong, H.; Wang, X. Geometry Processing of Dual Line Array Camera of GF-7 Satellite and Its Accuracy Verification. *J. Remote Sens.* **2024**, *28*, 756–766.
27. Zhang, Y. Research on 1:10,000 basic mapping based on Gaofen-7. *Geom. Spat. Inf. Technol.* **2024**, *47*, 218–220+224.
28. Zhou, Z.; Li, X.; Wu, P. A Combined Star Sensor/Gyro Satellite Attitude Determination Algorithm. *J. Ord. Equip. Eng.* **2021**, *42*, 187–191.
29. Zhu, Y.; Gao, J. Joint Filtering Orbiting Method Based on Dual Star Sensors/Gyroscopes. *J. Beijing Inf. Sci. Technol. Univ. Sci. Technol. Ed.* **2014**, *29*, 85–89.
30. Tang, H.; Xie, J.; Tang, X.; Chen, W.; Li, Q. On-Orbit Radiometric Performance of GF-7 Satellite Multispectral Imagery. *Remote Sens.* **2022**, *14*, 886. [CrossRef]
31. Mo, F.; Xie, J.; He, S.; Yin, S.; He, Y. Exploration on the pre-processing method of raw attitude data of Resource 3 satellite. *Sci. Surv. Map* **2016**, *41*, 127–132.
32. Xu, Y.; Chen, Q. Identification and Compensation of Thermal Variation Errors of Star Sensors in Satellite Attitude Determination. *Tech. Autom. Appl.* **2016**, *35*, 109–113.
33. Tong, X.; Ye, Z.; Li, L.; Liu, S.; Jin, Y.; Chen, P.; Xie, H.; Zhang, S. Detection and estimation of along-track attitude jitter from Ziyuan-3 three-line-array images based on back-projection residuals. *IEEE Trans. Geosci. Remote Sens.* **2017**, *55*, 4272–4284. [CrossRef]
34. Zhao, J. GF-7 Satellite Attitude Quality Evaluation and Accuracy Analysis. Master's Thesis, Liaoning Technical University, Fuxin, China, 2022.
35. Chen, L.; Letu, H.; Fan, M.; Shang, H.; Tao, J.; Wu, L.; Zhang, Y.; Yu, C.; Gu, J.; Zhang, N.; et al. An introduction to the Chinese high-resolution Earth observation system: Gaofen-1~7 civilian satellites. *J. Remote Sens.* **2022**, *2022*, 9769536. [CrossRef]

Disclaimer/Publisher's Note: The statements, opinions and data contained in all publications are solely those of the individual author(s) and contributor(s) and not of MDPI and/or the editor(s). MDPI and/or the editor(s) disclaim responsibility for any injury to people or property resulting from any ideas, methods, instructions or products referred to in the content.